Distributed Control of Low-Voltage Resistive AC Microgrids

Mohammad S. Golsorkhi, *Member, IEEE,* Qobad Shafiee, *Senior Member, IEEE,* Dylan D.C. Lu, *Senior Member, IEEE and* Josep M. Guerrero, *Fellow, IEEE*

***Abstract*— This paper proposes a distributed control strategy for coordination of distributed energy resources (DERs) in low-voltage resistive microgrids. The proposed framework consists of two level structures; primary and secondary control. Unlike the existing distributed control solutions, the proposed method is based upon the practical assumption of network impedance being resistive. The primary control level consists of a V-I droop mechanism, where GPS timing is used to synchronize the control agents. A consensus-based distributed secondary control method is introduced to improve the voltage regulation and load sharing accuracy of the V-I droop method. In the proposed approach, the *d*-axis component of the voltage is altered so as to regulate the average microgrid voltage to the rated value while guarantying proper sharing of active power among the DERs. Additionally, the *q*-axis component of voltage is adjusted to perform proper current and, accordingly reactive power sharing. The proposed control methodology accounts for the distribution line impedances. It features a plug-and-play environment; prior system knowledge is not required, and an arbitrary DER can enter the microgrid without any need for additional synchronization. An AC microgrid is prototyped to experimentally demonstrate the efficacy of the proposed method.**

***Index Terms*— Distributed control, dispersed storage and generation, microgrids, power sharing, voltage control.**

I. Introduction

The increased penetration of distributed energy resources (DERs) gives rise to new challenges in control, performance and power quality of distribution networks. A systematic approach towards the coordination of DERs is to view the DERs and associated loads as a microgrid (MG) [1]. Over the recent years, several cooperative control strategies including decentralized [2], [3], centralized [4], and distributed [5] approaches have been proposed for MGs. In the decentralized approaches, individual DERs are controlled by local controllers, which are often coordinated by using droop characteristics. Despite simple implementation, decentralized control methods suffer from voltage and frequency deviations and poor load sharing [6].

To overcome limitation of the decentralized methods and improve the performance, communication-based control schemes, including centralized and distributed approaches are introduced. While centralized methods favor high flexibility and performance [7], [8], they require an extensive and costly communication network to be implemented. In addition, a centralized controller suffers from single point-of compromise and failure [9]. To tackle these issues, distributed control architectures may be employed, in which the control objectives are realized through joint coordination of control agents [5], [10], [12]. Compared to the centralized control methods, distributed control schemes are more reliable and economical, but more difficult to analyze due to the complexity of the distributed dynamic systems.

Distributed control schemes are composed of local control agents interconnected through a sparse communication network. Each agent is assigned a set of information states, which express local variables e.g., average voltage, frequency or output power of the DER. By using a consensus control strategy, the local states reach a common value [13].

Over the recent years, several distributed control strategies have been proposed [5], [14]-[20]. In [5], a distributed control scheme comprising of primary and secondary control levels is presented. The primary controller adopts conventional active power-frequency (P-f) and reactive power-voltage (Q-V) droop characteristics to achieve proportional load sharing while ensuring stable operation, regardless of the availability of communication signals. A multi-agent structure is adopted in the secondary control layer to alleviate the frequency and voltage deviations while improving reactive power sharing among the DERs. This method is combined with a distributed averaging technique to reduce the communication requirements [14]. By modifying the secondary controller in [5], the resiliency of the method with respect to communication constraints [15], parameter uncertainty [16] and disturbances [17] are improved. Furthermore, by introducing an optimal controller in the secondary level, the stability of the MG is enhanced [18]. An optimal power flow-based control method is proposed in [19], where active power set points of the DERs is determined so as to minimize the total generation cost. A voltage droop control scheme is proposed in [20] to enhance the voltage profile by altering the active and reactive power generations of the DERs. However, the presented methods of [19] and [20] are designed for grid connected DERs but are not applicable to islanded MGs.

The methods of [5], [14]-[16], [18] use conventional droop mechanism in the primary level. Although the conventional droop scheme is simple and easy to implement, it suffers from slow dynamic response and is incompatible with the low inertia of the sources and low X/R ratio of network impedance in MGs. A solution is to utilize droop-free schemes, where the voltage and frequency are directly controlled by a distributed controller [21], [22]. However, the elimination of droop controller makes these methods vulnerable to communication interrupts. An alternative solution is proposed in [23], where the conventional droop is replaced by P-$\dot{V}$ and Q-f droop control scheme. Nevertheless, this scheme exhibits large transient oscillations following a load change, which can overload the DERs.

M.S. Golsorkhi is with the Department of Electrical and Computer Engineering, Isfahan University of Technology, Isfahan, IR 84156, Iran (email: golsorkhi@cc.iut.ac.ir). Q. Shafiee is with the Department of Electrical and Computer Engineering, University of Kurdistan, Sanandaj, Iran. Dylan D. C. Lu are with the School of Electrical and Information Engineering, University of Sydney, Camperdown NSW-2006, Australia. J. M. Guerrero are with the Institute of Energy Technology, Aalborg University, Aalborg East DK-9220, Denmark.

In this paper, which is an extension of the conference paper presented by the authors in [24], we introduce a distributed control framework which is in accordance with the inherent characteristics of inverter-based resistive MGs. In the primary level of the proposed framework, building on our recently introduced V-I droop control method [2], [25]-[28], a GPS based droop control method is adopted to alleviate the shortcomings of conventional droop method. The GPS timing technology enables synchronizing the reference frames of the individual control agents to a global synchronous rotating reference frame. Moreover, the global voltage regulation and active power sharing is ensured by adjusting the d-axis voltage, while the q-axis voltage is altered such that the load current and accordingly the reactive power are proportionally shared between the DERs.

The key feature of the proposed method is incorporation of the physical features of inverter-based MGs including, low X/R, lack of inertia and vulnerability of DERs to overcurrent in the control scheme. In particular,

- The existing distributed control methods [5], [14]-[18] control the frequency by introducing a virtual inertia in the inverter control loop. In addition, a frequency restoration mechanism is commonly adopted to compensate for frequency drifts. In the proposed method, however, inverters are synchronized to the synchronous reference frame, the frequency of which is constant. Therefore, frequency restoration is no longer necessary.
- The proposed scheme highlights the significance of current sharing as opposed to power sharing to prevent overcurrent stresses on inverter-based DERs. Specifically, the V-I droop controller, which is comprised of non-linear v_d-i_d and v_q-i_q droop characteristics, facilitates fast sharing of d and q axis current. In addition, the secondary controller adjusts the voltage offset of the droop controller to eliminate the current sharing error caused by the unknown line impedances.
- To make the most of capacity of lightly loaded inverters for reactive power generation, the q-axis current of each unit is adjusted based on the available capacity of the inverter for reactive power generation. Therefore, a unit with high active power loading generates a smaller reactive power compared to a similar unit with low active power output.
- The proposed method offers a plug-and-play scheme, which allows connection of a new DER to the system without requirement of any information about the MG parameters, changing the overall control structure.

The rest of this paper is organized as follows. Section II describes the conventional and V-I droop control schemes for microgrids. The proposed control method is detailed in Section III. In Section IV, the mathematical model of the proposed framework is derived and used to analyze the small signal stability. Experimental results are presented in Section V. Section VI concludes the paper.

II. Droop Control Scheme

Droop control schemes are commonly used in practice to maintain load/generation balance while regulating the voltage and frequency. Assuming inductive network impedance, the active and reactive powers are proportional with the angle and magnitude of the voltage, respectively. This relationship is used as the basis of the conventional droop method, in which the dispatchable DER units are coordinated according to the P-f and Q-V droop characteristics. However, this assumption is not practical for low voltage MGs, in which the R/X ratio is as large as seven [29]. Additionally, the conventional droop suffers from slow dynamics as well as frequency and voltage fluctuations, which degrade the power quality.

To enhance the performance of the conventional droop method, several modified power-droop schemes including, P-V and Q-f droop [30], P-$\dot{V}$ and Q-f droop [23], virtual impedance [31] and adaptive droop [32] schemes have been proposed in the literature. An alternative approach presented in [2] achieves a fast dynamic response by directly controlling the inverter voltage according to the output current. In this scheme, the dq reference frames of all DERs are synchronized with a global frame by means of GPS timing technology. This way, all DERs will operate at fixed frequency; hence the frequency fluctuations are eliminated. Furthermore, the inverter reference voltage (v^*), is controlled, according to the droop control law:

$$\begin{bmatrix} v_d^* \\ v_q^* \end{bmatrix} = \begin{bmatrix} E_0 \\ 0 \end{bmatrix} - \begin{bmatrix} r_d g(i_d) \\ r_q i_q \end{bmatrix} + \begin{bmatrix} R_{gs} & -X_{gs} \\ X_{gs} & R_{gs} \end{bmatrix} \begin{bmatrix} i_d \\ i_q \end{bmatrix} \quad (1)$$

where i , E_0 , R_{gs} , X_{gs} , r_d , r_q and g are the output current, rated voltage, grid side inductor resistance and reactance, d-axis and q-axis droop coefficients, and droop function, respectively.

The second term on the right hand side (RHS) of (1) is the droop signal, which adjusts the d and q axis components of the voltage according to v_d-i_d and v_q-i_q droop characteristics, respectively. The droop function, $g(\cdot)$, is a monotonic peicewise linear function, which is introduced to improve the sharing accuracy at high loading conditions. To mitigate the adverse effect of grid side inductor (transformer) on the voltage regulation and power sharing, a compensation term is added on the RHS of (1).

Equation (1) indicates that the voltage phasor is almost aligned with the d-axis. Assuming the voltage variations are small throughout the MG, P and Q are proportional with i_d and i_q, respectively. Therefore, the active and reactive power can be proportionally shared among the DERs by selecting the droop coefficients as [33]

$$r_{d1}P_{r,1} = r_{d2}P_{r,1} = \cdots = r_{dn}P_{r,n} \quad (2)$$

$$r_{q1}Q_{r,1} = r_{q2}Q_{r,2} = \cdots = r_{qn}Q_{r,n} \quad (3)$$

in which $P_{r,i}$ and $Q_{r,i}$ refer to the rated active and reactive power of DER unit i, respectively.

Since the aforementioned V-I droop control scheme relies on GPS signal at the DER local controllers, the robust V-I /Q-f droop control scheme proposed in [27] may be employed in practice to ensure stable operation in case of GPS failure.

The schematic diagram of the primary control scheme is illustrated in Fig. 1. The V-I droop controller obtains the inverter reference voltage (v^*), according to (1). In order to track the reference voltage with zero steady state error, a cascaded voltage-current control loop is implemented using proportional resonant (PR) controllers. The output of the cascaded control loop is used as the reference signal for PWM switching scheme, which determines the switching state of the inverter.

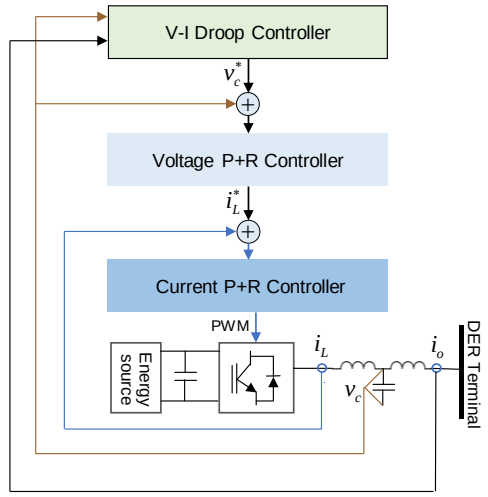

Fig. 1. V-I droop-based primary control scheme.

III. Problem Statement

The operation of the V-I control scheme is demonstrated based on Fig. 2. A microgrid consisting of two parallel DERs with the same power rating connected to a point of common coupling (PCC) is considered. To simplify the analysis, the lines connecting the DERs to the PCC are assumed to be purely resistive in this Section. It is worth mentioning that this assumption is an approximation of the distribution line impedances, where R/X ratio is large, Nevertheless, the application of the proposed method is not limited to purely resistive networks, as demonstrated in Sections V and VI.

Consider the case that the resistance of line 2 (R_{L2}) is larger than line 1 (R_{L1}). The v_d-i_d droop characteristics for the two DER units are depicted in Fig. 2(a). It can be seen that due to the mismatch between the line impedances, unit 1 supplies a larger q-axis current compared to unit 2. In case of v_q-i_q droop characteristics (Fig. 2(b)), the offset voltage of both units is equal to the rated voltage (E_0). Since the line impedance of unit 1 is smaller than unit 2, the d-axis output current of unit 1 is larger. Additionally, the d-axis voltages of both units are deviated from the nominal value.

The above demonstration shows that the sharing accuracy of the V-I droop mechanism is dependent on the line impedances and the distribution of the load in the MG. In addition, the voltage deviations caused by the droop characteristics degrades the voltage regulation across the MG. One can note that similar sharing mismatch exists in case of conventional P-f and Q-E droop method. In the next Section, a distributed control scheme is proposed to improve the sharing accuracy and voltage regulation of the V-I droop mechanism.

IV. Proposed Solution

In order to enhance the sharing accuracy and voltage regulation of the V-I droop scheme, the v_d-i_d and v_q-i_q droop curves of individual DERs are modified by adding appropriate voltage offsets, i.e.,

$$\begin{bmatrix} v_d^* \\ v_q^* \end{bmatrix} = \begin{bmatrix} E_0 \\ 0 \end{bmatrix} - \begin{bmatrix} r_d g(i_d) \\ r_q i_q \end{bmatrix} + \begin{bmatrix} R_{gs} & -X_{gs} \\ X_{gs} & R_{gs} \end{bmatrix} \begin{bmatrix} i_d \\ i_q \end{bmatrix} + \begin{bmatrix} v_{sd} \\ v_{sq} \end{bmatrix} \quad (4)$$

in which v_{sd} and v_{sq} are the d and q axis voltage correction terms, respectively.

As shown in Fig. 3, equal sharing of iq is achieved by application of a positive offset voltage (v_{sq2}) to the vq-iq droop

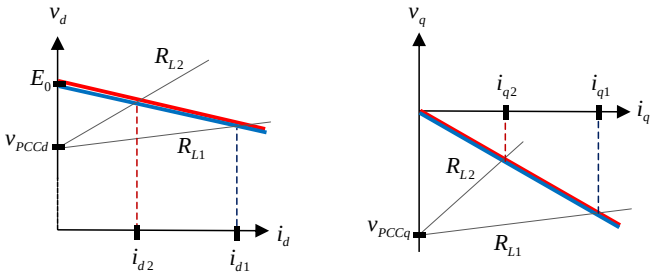

Fig. 2. Principle of V-I droop mechanism.

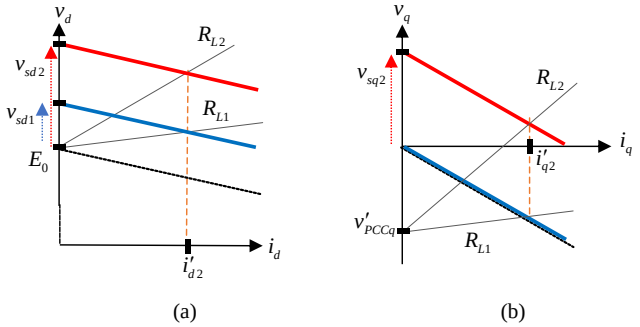

Fig. 3. Effect of secondary controller on V-I droop characteritics: a) d-axis, b) q-axis.

characteristic of unit 2. In case of *vd-id* droop characteristic, the droop curves of both units are added with a positive shift, to compensate the voltage deviation at the PCC. However, the voltage offset of unit 2 (v_{sd2}) must be larger than the voltage offset of unit 1 (v_{sd1}) to guarantee equal sharing of the d-axis currents despite unequal line resistances.

The d and q axis voltage correction terms are obtained using a distributed control scheme, as depicted in Fig. 4. In this scheme, the local secondary controllers of individual DERs, which are referred to as control agents, are interconnected through a cyber network to allow information exchange between the neighbor units. These agents are coordinated based on the consensus concept. In this scheme, an information state, x_i, is assigned to each control agent (i.e., the local secondary controller). The information states are shared between the agents through a sparse communication network. The state of each agent is updated based on the received information form the neighbors. If the distributed communication network contains minimum connectivity, all of the states will converge to a common value, e.g., the average of initial states [34].

In the following subsections, two different control methods are presented to achieve the objectives of proportional load sharing and voltage regulation based on the consensus concept.

A. Proportional Current Sharing

The problem of proportional load sharing among DERs is simplified to the subproblems of proportional sharing of d-axis and q-axis currents. In the framework of consensus protocol, the proportional sharing of i_d can be interpreted as enforcing the per unit d-axis currents of the individual units to reach a common value,

$$\frac{i_{d,1}}{i_{d,1}^{rated}} = \frac{i_{d,2}}{i_{d,2}^{rated}} = \cdots = \frac{i_{d,n}}{i_{d,n}^{rated}} \quad (5)$$

where $i_{d,i}^{rated}$ denotes the rated d-axis current of DER unit i.

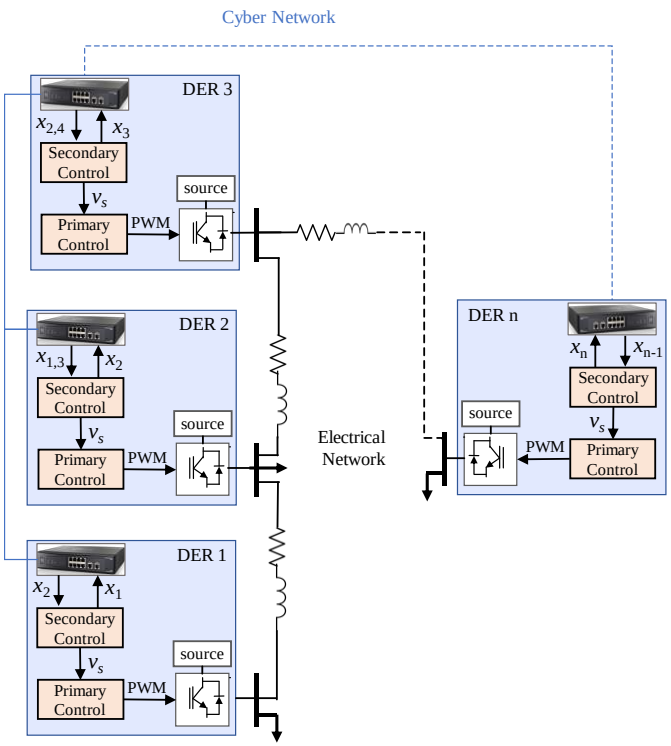

Fig. 4. General scheme of the proposed distributed control framework.

In order to achieve (5), the *d*-axis voltage correction term of unit *i* is updated according to the difference between the per unit *d*-axis currents of unit *i* and its neighbor units as

$$v_{sd,i} = \frac{k_d}{s}\sum_{j\in N_i}\left(\frac{i_{d,j}}{i_{d,j}^{rated}} - \frac{i_{d,i}}{i_{d,i}^{rated}}\right) \tag{6}$$

in which *s* is the derivative operator, k_d is the *d*-axis consensus controller gain. Furthermore, N_i refers to the set of neighbors of agent *i*, i.e., the set of units which are interconnected with DER i through a communication link.

Similarly, the *q*-axis voltage correction term is updated as

$$v_{sq,i} = \frac{k_q}{s}\sum_{j\in N_i}\left(\frac{i_{q,j}}{i_{q,j}^{rated}} - \frac{i_{q,i}}{i_{q,i}^{rated}}\right) \tag{7}$$

where k_q is the *q*-axis consensus controller gain.

Equations (6) and (7) denote that the *d* and *q* axis voltage correction terms are changed so as to reduce the mismatch between the per unit *d* and *q* axis currents of each DER with its neighbors. Assuming a stable distributed control system, the current sharing mismatch will reach zero in steady-state.

The distributed control algorithm must compensate the voltage deviations caused by the droop controller and line voltage drops. To that end, a voltage compensation term is added to the right-hand side of (6),

$$v_{sd,i} = \frac{k_v}{s}\left(E_0 - \overline{v}_i\right) + \frac{k_d}{s}\sum_{j\in N_i}\left(\frac{i_{d,j}}{i_{d,j}^{rated}} - \frac{i_{d,i}}{i_{d,i}^{rated}}\right) \tag{8}$$

where $\overline{v}_i$ is the average MG voltage across the DER buses estimated by unit *i*, which is obtained by using the distributed averaging technique called dynamic consensus [35],

$$\dot{\overline{v}}_i = v_i + \frac{k_{avg}}{s}\sum_{j\in N_i}\overline{v}_j - \overline{v}_i, \tag{9}$$

where k_{avg} is the integral gain, N_i is the set of neighbors of agent *i*, and v_i is the local terminal voltage, v_i.

To avoid the obligation to add another sensor for measurement of DER terminal voltage, this signal is estimated using the capacitor voltage, v_{dq}, and the output current, i_{dq}, as

$$v_{dq} = v_{cdq} + \begin{bmatrix} R_{gs} & -X_{gs} \\ X_{gs} & R_{gs} \end{bmatrix} i_{dq} \tag{10}$$

$$v = G_{LPF}(s)\sqrt{v_d^2 + v_q^2} \tag{11}$$

in which $G_{LPF}(s)$ is a first order low-pass filter, with cutoff frequency ω_c,

$$G_{LPF}(s) = \frac{\omega_c}{s + \omega_c} \tag{12}$$

B. Proportional Active Power/rms Current Sharing

The control method proposed in Section III-A attempts to achieve proper load sharing through proportional sharing of *d* and *q* axis currents. However, the load sharing accuracy of that method may be affected by the dependency of active power on the DER terminal voltage, which varies throughout the MG. To enhance the active power sharing accuracy, an alternative method is presented.

Here, the *d*-axis voltage correction term, v_{sd}, is defined as the combination of a voltage compensation term and an active power-sharing term, as follows:

$$v_{sd,i} = \frac{k_v}{s}\left(E_0 - \overline{v}_i\right) + \frac{k_P}{s}\sum_{j\in N_i}\left(\frac{p_j}{P_{r,j}} - \frac{p_i}{P_{r,i}}\right) \tag{13}$$

in which k_P is the power controller gain. The active power is calculated using

$$p = G_{LPF}(s)\left(v_d i_d + v_q i_q\right) \tag{14}$$

Equation (13) implies that the control agents regulate the average voltage at the rated value while attempting to achieve proportional active power sharing.

Since the safe operation region of the DERs is limited by their output current rather than a maximum reactive power, rms output current of the DERs must be considered as the key factor in reactive power allocation. A current-based reactive power sharing mechanism is proposed to prevent the DERs from overcurrent stress. In this scheme, the normalized value of the *q*-axis current of the DER and its neighbors are compared to find the loading mismatch. By controlling the secondary voltage, v_{sq}, according to the following consensus law, the current mismatch in steady-state can be reduced.

$$v_{sq,i} = \frac{k_q}{s}\sum_{j\in N_i}\left(i_{qn,j} - i_{qn,i}\right) \tag{15}$$

The normalized *q*-axis current, i_{qn}, is defined as

$$i_{qn} = G_{LPF}(s)\frac{i_q}{I_q^{\max}} \tag{16}$$

in which $I_q^{\max}$ is the maximum permissible *q*-axis current.

To prevent overcurrent stress on the DER, the rms output current must be limited to bellow the rated value. The rms current is related to the *d* and *q*-axis components according to:

$$i_{rms} = \frac{1}{\sqrt{3}}\sqrt{i_d^2 + i_q^2} \tag{17}$$

A practical solution for preventing rms current overload during high loading conditions is altering the reactive power sharing among the DERs in such a way that the units which generate a higher active power (i_d) produce less reactive power (i_q) compared to the lightly loaded units. This strategy can be embedded into the proposed control scheme by adjusting the maximum *q*-axis current as

$$I_q^{\max} = \sqrt{I_{rated}^2 - i_d^2} \tag{18}$$

in which I_{rated} refers to the rated current in *d*-*q* frame, i.e., $\sqrt{3}$ times the nominal rms current.

Equation (18) implies that as the *d*-axis current of a DER increases, its available capacity for *q*-axis current generation drops. In contrast with the conventional reactive power sharing methods, the proposed scheme increases the contribution of lightly loaded DERs in supplying the reactive power demand. As a result, the rms current of highly loaded units falls and thus overloading is prevented. In addition, the proposed method directly controls the current rather than reactive power. This strategy is in accordance with the fact that the DERs' safe operating region is determined by maximum rms current.

C. Extension of the Method to Renewable Energy Resources

Similar to the conventional droop mechanism, the V-I droop strategy is developed for dispatchable energy resources (e.g. battery storage, micro-turbines), which can change their power generation in response to load demand variations. The output power of PV and wind-based renewable energy resources (RESs) are commonly determined based on maximum power point tracking (MPPT) algorithm rather than the loading conditions. Thus, the inverter stage of an RES is typically operated in current controlled mode, with *d*-axis component of the reference current being controlled according to the MPPT and the *q*-axis component of the current regulated at zero to ensure unity power factor [36].

In this paper, the proposed control method is extended to RESs to enable the participation of these units in reactive power generation. In the proposed solution, the *q*-axis voltage is calculated as a combination of the V-I droop mechanism and the secondary control scheme, i.e.,

$$v_q^* = X_{gs} i_d - \left(r_q - R_{gs}\right) i_q + v_{sq} \tag{19}$$

in which v_{sq} is obtained from consensus control scheme in (15). The difference between the reference and the measured *q*-axis voltage is passed through a PI controller to generate the *q*-axis current set-point, used as a reference for the current control.

V. Mathematical Analysis of The Proposed Method

In this section, a state-space model of the MG with the proposed control method is developed. By application of the model to a test MG, small signal analysis is carried out to investigate the dynamic response of the proposed strategy and provide a guideline for the controller design.

A. State-space Model

The dynamic response of the average voltage estimation policy can be expressed in matrix form, as [22]

$$\bar{\boldsymbol{v}} = -k_{avg}\boldsymbol{L}\int \bar{\boldsymbol{v}}\left(\tau - T_d\right)d\tau + \boldsymbol{v} \tag{20}$$

in which $\boldsymbol{v} = [v_1, v_2, \cdots, v_n]$ and $\bar{\boldsymbol{v}} = [\bar{v}_1, \bar{v}_2, \cdots, \bar{v}_n]$ are the vectors of measured voltages and estimated average voltages, respectively. Furthermore, T_d is the communication delay, $\boldsymbol{I}$ is the identity matrix and $\boldsymbol{L}$ is the Laplacian matrix of the communication network. Defining $\boldsymbol{w} = \int\left(\bar{\boldsymbol{v}}(\tau) - \boldsymbol{E_0}\right)d\tau$, where $\boldsymbol{E_0}$ is a column vector with elements E_0, one can arrange (20) in state-space form, as

$$\frac{d}{dt}\boldsymbol{w} = -k_{avg}\boldsymbol{L}\boldsymbol{w}\left(t - T_d\right) + \boldsymbol{v} - \boldsymbol{E_0} \tag{21}$$

Additionally, the global dynamic response of the d and q axis controllers can be expressed in matrix form, as follows:

$$\frac{d}{dt}\boldsymbol{v_{sd}} = k_v\left(\boldsymbol{E_0} - \bar{\boldsymbol{v}}\right) - k_P\boldsymbol{L}\boldsymbol{P_r^{-1}}\boldsymbol{p}\left(t - T_d\right) \tag{22}$$

$$\frac{d}{dt}\boldsymbol{v_{sq}} = -k_q\boldsymbol{L}\boldsymbol{i_{qn}}\left(t - T_d\right) \tag{23}$$

where $\boldsymbol{v_s}$, $\boldsymbol{p}$, $\boldsymbol{i}$, $\boldsymbol{i_{qn}}$ are the vectors of secondary voltages, active powers, output currents and normalized *q* axis currents of the DERs, respectively. Moreover, $\boldsymbol{P_r}$ is a diagonal matrix containing the power ratings of the DERs. Using (21) and (22), the derivative of vsd can be written as:

$$\frac{d}{dt}\boldsymbol{v_{sd}} = k_v k_{avg}\boldsymbol{L}\boldsymbol{w}\left(t - T_d\right) - k_v\boldsymbol{v} + k_v\boldsymbol{E_0} - k_P\boldsymbol{L}\boldsymbol{P_r^{-1}}\boldsymbol{p}\left(t - T_d\right) \tag{24}$$

The rank of Laplacian matrix is (*n*-1) and its last column is equal to the summation of the columns 1 to *n*-1. In order to avoid eigenvalues at the origin, it is possible to reduce the order of the system by defining the auxiliary states $\boldsymbol{v_{auxd}}$ and $\boldsymbol{v_{auxq}}$, as:

$$\boldsymbol{v_{aux}} = \begin{bmatrix} v_{sd1} - v_{sdn} \\ \vdots \\ v_{sd,n-1} - v_{sdn} \\ v_{sq1} - v_{sqn} \\ \vdots \\ v_{sq,n-1} - v_{sqn} \end{bmatrix}_{2n-2} \tag{25}$$

Combining (21)-(25), the secondary controller can be shown in state-space form, as

$$\begin{bmatrix} \dot{\boldsymbol{w}} \\ \dot{\boldsymbol{v}}_{\boldsymbol{saux}} \end{bmatrix} = A_{sd}\begin{bmatrix} \boldsymbol{w}\left(t - T_d\right) \\ \boldsymbol{v_{saux}}\left(t - T_d\right) \end{bmatrix} + B_s\begin{bmatrix} \boldsymbol{v} \\ \boldsymbol{p} \\ \boldsymbol{i_{qn}} \end{bmatrix} + B_{sd}\begin{bmatrix} \boldsymbol{v}\left(t - T_d\right) \\ \boldsymbol{p}\left(t - T_d\right) \\ \boldsymbol{i_{qn}}\left(t - T_d\right) \end{bmatrix} + \begin{bmatrix} \boldsymbol{E_0} \\ 0 \\ 0 \end{bmatrix} \tag{26}$$

$$\boldsymbol{v_{sdq}} = C_s\begin{bmatrix} \hat{\boldsymbol{w}} & \hat{\boldsymbol{v}}_{\boldsymbol{saux}} \end{bmatrix}^T \tag{27}$$

The calculation block and the associated low-pass filters are formulated as a set of nonlinear differential equations, as

$$\frac{1}{\omega_c}\frac{d}{dt}p = -p + i_d v_d + i_q v_q \tag{28}$$

$$\frac{1}{\omega_c}\frac{d}{dt}v = -v + \sqrt{v_d^2 + v_q^2} \tag{29}$$

$$\frac{1}{\omega_c}\frac{d}{dt}i_{qn} = -i_{qn} + \frac{i_q}{\sqrt{I_{rated}^2 - i_d^2}} \tag{30}$$

The primary control level and LCL filter of each DER can be expressed as an eights-order dynamic system [37]. Since the dynamics of the secondary control level is much slower compared to the primary control level, it is reasonable to use a reduced order model for the primary control level which neglects the high frequency modes. , i.e.,

$$\frac{1}{b}\frac{d}{dt}v_{dq} = -v_{dq} + v_{dq}^{*} \tag{31}$$

in which b is the reciprocal of the time constant.

Combining (28)-(31) and (4), and linearizing around the equilibrium point, the linearized model for the primary control and measurement block of DER i is obtained as

$$\frac{d}{dt}\begin{bmatrix}\hat{v}_d\\ \hat{v}_q\\ \hat{v}\\ \hat{p}\\ \hat{i}_{qn}\end{bmatrix} = \begin{bmatrix} -b & 0 & 0 & 0 & 0\\ 0 & -b & 0 & 0 & 0\\ \omega_c V_d/V & \omega_c V_q/V & -\omega_c & 0 & 0\\ \omega_c I_d & \omega_c I_q & 0 & -\omega_c & 0\\ 0 & 0 & 0 & 0 & -\omega_c\end{bmatrix}\begin{bmatrix}\hat{v}_d\\ \hat{v}_q\\ \hat{v}\\ \hat{p}\\ \hat{i}_{qn}\end{bmatrix} + \begin{bmatrix} b & 0\\ 0 & b\\ 0 & 0\\ 0 & 0\\ 0 & 0\end{bmatrix}\begin{bmatrix}\hat{v}_{sd}\\ \hat{v}_{sq}\end{bmatrix} + \begin{bmatrix} b(-r_d g'(i_d) + R_{gs}) & -bX_{gs}\\ bX_{gs} & b(-r_q + R_{gs})\\ 0 & 0\\ \omega_c V_d & \omega_c V_q\\ I_d I_q \omega_c \left(I_{rated}^2 - I_d^2\right)^{-3/2} & \omega_c \left(I_{rated}^2 - I_d^2\right)^{-1/2}\end{bmatrix}\begin{bmatrix}\hat{i}_d\\ \hat{i}_q\end{bmatrix} \tag{32}$$

Expanding (32), the dynamics of the primary controllers of all of the DERs can be expressed in the matrix form,

$$\dot{x}_p = A_p x_p + B_{p1}\begin{bmatrix}\hat{\boldsymbol{v}}_{\boldsymbol{sd}}\\ \hat{\boldsymbol{v}}_{\boldsymbol{sq}}\end{bmatrix} + B_{p2}\begin{bmatrix}\hat{\boldsymbol{i}}_{\boldsymbol{d}}\\ \hat{\boldsymbol{i}}_{\boldsymbol{q}}\end{bmatrix} \tag{33}$$

where $x_p = \begin{bmatrix}\hat{\boldsymbol{v}}_{\boldsymbol{d}} & \hat{\boldsymbol{v}}_{\boldsymbol{q}} & \hat{\boldsymbol{v}} & \hat{\boldsymbol{p}} & \hat{\boldsymbol{i}}_{\boldsymbol{qn}}\end{bmatrix}^T$.

The distribution network and associated loads can be represented in terms of an admittance matrix. Using Kron reduction, the output currents of the DER can be expressed in terms of the DER output voltages [38]:

$$\boldsymbol{i}_{\boldsymbol{dq}} = Y\boldsymbol{v}_{\boldsymbol{dq}} \tag{34}$$

where Y is the reduced order admittance matrix of the network. Substituting (34) into (33) yields

$$\dot{x}_p = \left(A_p + B_{p2} Y\begin{bmatrix} I_{2N} & \mathbf{0}_{2N*3N}\end{bmatrix}\right)x_p + B_{p1}\begin{bmatrix}\hat{\boldsymbol{v}}_{\boldsymbol{sd}}\\ \hat{\boldsymbol{v}}_{\boldsymbol{sq}}\end{bmatrix} \tag{35}$$

Furthermore, the inputs of the proposed secondary control strategy are related to the states of the primary control level, as follows:

$$\begin{bmatrix}\hat{\boldsymbol{v}}\\ \hat{\boldsymbol{p}}\\ \hat{\boldsymbol{i}}_{\boldsymbol{qn}}\end{bmatrix} = \begin{bmatrix}\mathbf{0}_{3N*2N} & I_{3N}\end{bmatrix}x_p = C_p x_p \tag{36}$$

Combining the state space equations of the secondary control level ((26), (27)) with the primary control level ((35), (36)), the state matrix of the entire MG is obtained as

$$\begin{bmatrix}\dot{x}_p\\ \dot{x}_s\end{bmatrix} = \begin{bmatrix} A_p + B_{p2} Y\begin{bmatrix} I & 0\end{bmatrix} B_{p1} C_s & \\ B_s C_p & 0\end{bmatrix}\begin{bmatrix}x_p\\ x_s\end{bmatrix} + \begin{bmatrix} 0 & 0\\ B_{sd} C_p & A_{sd}\end{bmatrix}\begin{bmatrix}x_p(t - T_d)\\ x_s(t - T_d)\end{bmatrix} \tag{37}$$

where $x_s = \begin{bmatrix}\hat{\boldsymbol{w}} & \hat{\boldsymbol{v}}_{\boldsymbol{saux}}\end{bmatrix}^T$.

B. Small Signal Analysis

Equation (37) is a delay differential equation with a single delay (T_d). The system characteristic equation is represented as [38]

$$\det\left(-sI + A + A_d e^{-sTd}\right) = 0 \tag{38}$$

where A and A_d are the first and second matrix on the right-hand side of (38). Several approaches are proposed in applied mathematics literature for solving (38), among which infinitesimal generator discretization is considered as the most straightforward one [39]. This method is conveniently implemented in MATLAB using two lines of code [40].

The loci of the system eigenvalues for a test MG (detailed in Section VI) with respect to variations of communication delay (Td), the proposed controller's gain, k_p, and MG load are illustrated in Fig. 5. In this figure, "x" shows the locus of eigenvalues corresponding with minimum value of the parameter and red arrows show the direction of movement with the increase of the parameter.

In Fig. 5(a), the communication delay is changed from 50ms to 55ms. It is observed that the medium frequency eigenvalues (with real parts ranging from -60rad/s to -30rad/s) move towards the origin. Furthermore, low-frequency eigenvalues (with real parts between -20 and -10 rad/s) move towards each other. When the delay is increased further (See Fig. 5(b)), the high frequency eigenvalues move towards the origin and the low frequency modes move towards the imaginary axis. As a result, the system will experience low frequency oscillations with low damping ratio. It is worth mentioning that the maximum time delay for stable operation depends on the control parameters. Therefore, stable operation in the presence of an arbitrary communication delay can be guaranteed by selecting appropriate control parameters.

The effect of variations of parameters k_p, k_q and k_v, is illustrated in Figs. 5(c)-(e), respectively. In these figures, k_p, k_q and k_v are changed within the ranges (30, 300), (20, 200), and (2, 20), respectively. From Fig. 5(c), it is observed that for smaller values of k_p the real parts of the dominant modes increase, which implies a faster dynamic response. For large values of k_p, however, the dominant modes become oscillatory. Similar phenomenon occurs when k_q is increased. In case of k_v, however, the trajectory of eigenvalues is slightly different. Specifically, while the increase of k_p and k_q causes the low frequency eigenvalues to become unstable, the parameter k_v has a destabilizing effect on the medium frequency eigenvalues. The reason is that k_p and k_q act on d and q axis current sharing, which is primarily controlled by V-I droop scheme whereas k_v directly changes the d-axis voltage. As a consequence, the modes which are related to k_v have a higher imaginary frequency compared to the modes related to k_p and k_q. This analysis is used as the basis for the design of control parameters in the experimental implementation.

The effect of variations of the load is demonstrated in Fig. 5 (f) of the revised paper and also shown below. It is seen that as the load is changed between 1% to 100% of the MG capacity,

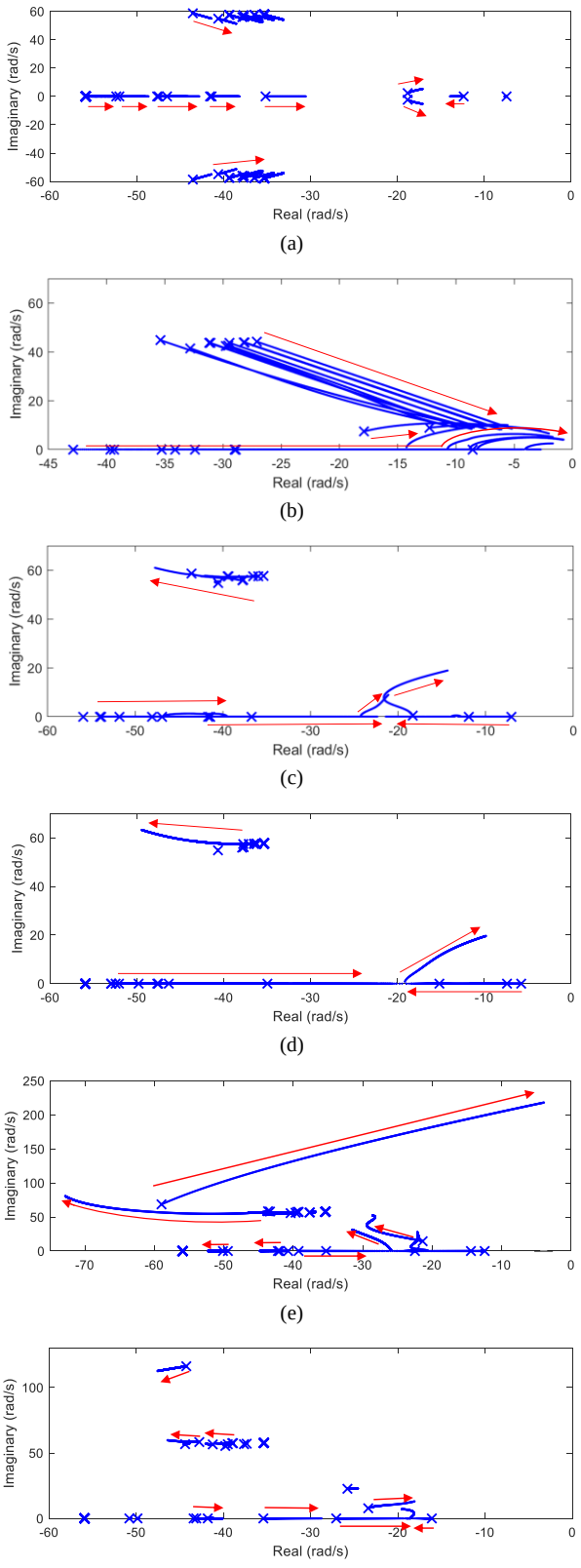

Fig. 5. Loci of system eigenvalues: a) T_d changes from 50ms to 55ms, b) T_d changes from 65ms to 250ms, c) k_p changes from 30 to 300, d) kq changes from 20 to 200, e) kv changes from 2 to 20, f) load changes between 1-100%

the dominant eigenvalues move away from the imaginary axis but some of the eigenvalues slightly move towards the imaginary axis. Nevertheless, the system remains stable regardless of the load variations.

The controller design is carried out in two stages. Firstly, the time delay is set at the typical expected value and the control parameters are selected such that a desirable damping is achieved. Secondly, the time delay is increased to the maximum estimated value to check the system stability. If the system is unstable, the damping ratio will be deceased and the design process is repeated until the stability is guaranteed.

TABLE I. ELECTRICAL AND CONTROL PARAMETERS OF THE TEST MG

Parameter	Symbol	Value
Nominal phase voltage	E_0	220 Vrms
Nominal Frequency	f_r	50 Hz
Inverter nominal power	P_r	1500 W
LCL filter parameters	L_{cs}/ C / L_{qs}	8.6 mH / 4.5μF / 1.8mH
Line impedance	Z_{L1}	0.66+ j0.07
	Z_{L2}	0.5+ j0.07
	Z_{L3}	0.5+ j0.07
Load impedances (case 1)	Z_{Load1}/ Z_{Load2}	35Ω/ 35+j40 Ω
Load impedances (case 2)	Z_{Load1}/ Z_{Load2}	57Ω/ 34+j47 Ω
Communication rate	f_{com}	100 samples/s
Communication delay	T_d	10 ms
DSC parameters	k_{avg}	1.2 s^{-1}
	k_v	6 s^{-1}
	k_p	60 s^{-1}
	k_q	90 Ω $-s^{-1}$
Droop coefficients	r_d	5.5 Ω
	r_q	20 Ω

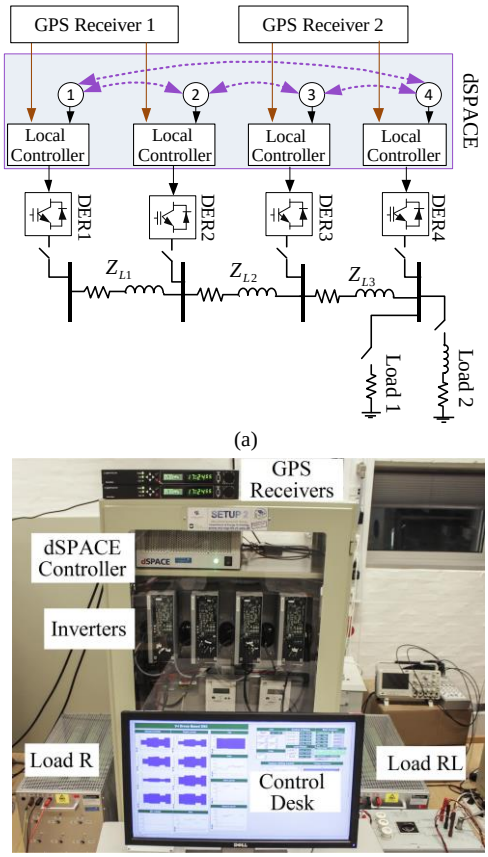

Fig. 6. Experimental setup: a) schematic diagram and b) hardware prototype.

VI. EXPERIMENTAL RESULTS

The proposed method was implemented on a MG test bed, shown in Fig. 6. The test bed was prototyped in the Intelligent Microgrid Laboratory at Aalborg University [41]. The test setup is composed of four inverter-based DER units, which are supplied by a programmable DC source. While DERs 2-4 serve as dispatchable sources which can change their active power generation depending on the load demand, DER 1 emulates an RES generation which operates at its maximum power point. The electrical and control parameters are listed in TABLE I.

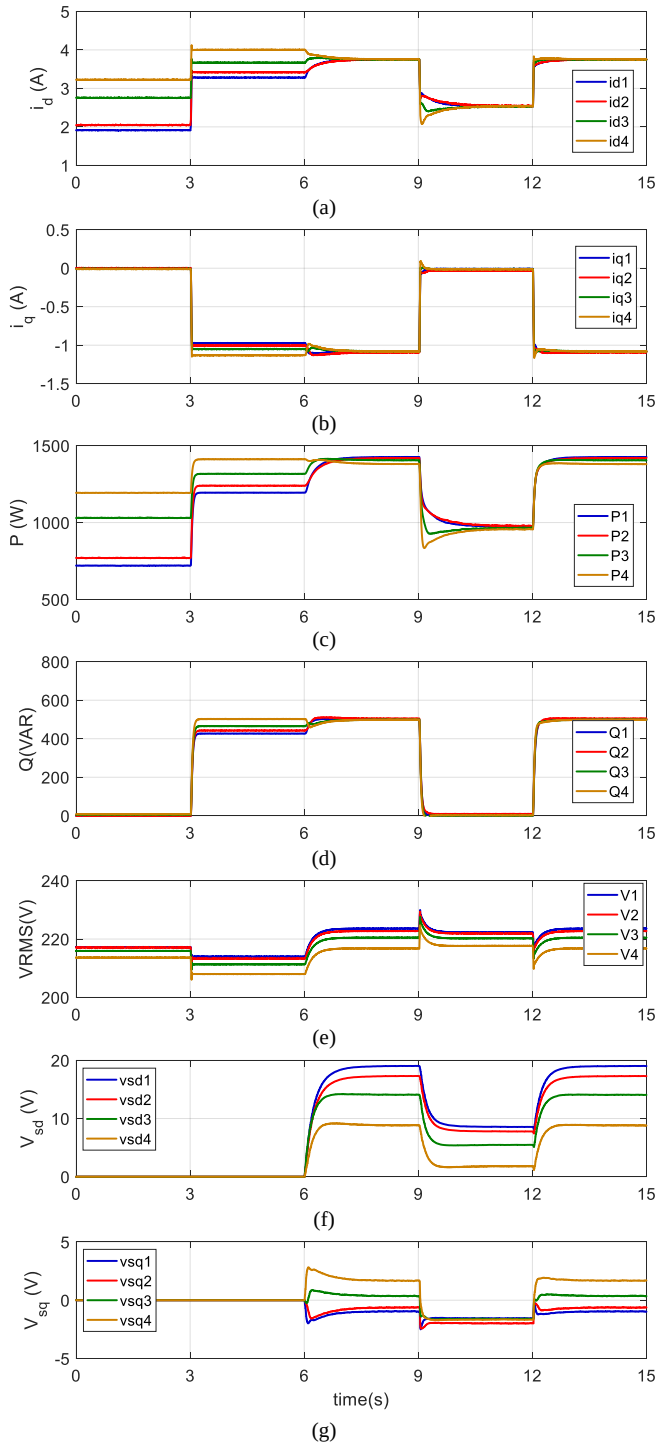

Fig. 7. Performance of the proposed control method in Section IV-A: a) d-axis currents, b) *q*-axis currents, c) active powers, d) reactive powers, e) rms voltages.

It is worth mentioning that, the v_d-i_d and v_q-i_q droop characteristics employ piecewise linear curves, in which the slope of the line segments increases with the increase of current. This way, the effect of line impedance on sharing accuracy is attenuated at high loading conditions, hence achieving a better sharing accuracy when the system is near full load [2].

Each DER unit is controlled by a local controller. A ring-shaped communication network (shown as broken lines) is used to enable information exchange between the neighbor DER units. The proposed control routine is implemented in a dSPACE 1006 digital control system. To consider the communication constrains, each of the communication links is emulated in dSPACE as low bandwidth link with data rate of 100 samples per second and delay of 10ms. Two Spectracom ® GPS synchronization systems [42] are used to synchronize the local controllers with the UTC.

The DER units are interconnected through a line model. The R/X ratio of the lines are selected in accordance with the practical distribution systems [29]. The MG loads are modeled by a combination of resistive and inductive loads.

To validate the efficacy of the proposed method, four case studies are presented; dynamic performance assessment of methods A and B, resilience of the method to communication constraints, and plug'n'play capability. The experimental results are captured using dSPACE Control Desk and plotted in MATLAB.

A. Performance of Current Sharing Control Method

The dynamic performance of the current sharing control method proposed in Section IV-A is demonstrated in the experimental results of Fig. 7. Initially, load 1 is connected and the distributed secondary controller (DSC) is disabled, hence the load demand is shared among DERs according to the V-I droop characteristics. However, the sharing is not accurate due to the voltage deviations across the feeder. Specifically, DER4 provides the largest share (id4) due to its electrical closeness with the load.

At $t = 3s$, Load 2 is plugged in. As shown in Fig. 7(a), the load sharing accuracy is improved at higher loading conditions thanks to the piece linear droop charactersitic. Nevertheless, a considerable error is observed in both *d* and *q* axis current sharing. Additionally, the voltage of DER4 (V4) falls to 210V (see Fig. 7(e)).

Subsequent to activation of the DSC at $t = 6\text{s}$, the *d*-axis secondary signals are increased to positive values to compensate the voltage deviations while eliminating *d*-axis current sharing errors (see Fig. 7(f)). Specifically, vsd1 is increased above vsd2-vsd4 to increase the share of unit 1 from the load active power. Similarly, the *q*-axis secondary signals are changed to achieve equal sharing of *q*-axis current. Load 2 is turned off and on at $t = 9\text{s}$ and 12 s, respectively. It is observed that the i_d and i_q are shared accurately among the DERs and the voltages remain within the permissible range during the transients. However, there still exits some inaccuracy in active power sharing due to the variations of voltage throughout the MG.

B. Performance of P/Irms Sharing Control Method

The performance of P/Irms control method (Section IV-B) is illustrated in Fig. 8. In this case, DER 1 is assumed to be a DER with initial power generation of 200W. Prior to activation of DSC at t=6s, the V-I droop controls the power sharing among the units.

In order to ensure proper sharing of active and reactive power, the secondary control method presented in Section IV-B is activated at $t = 6\text{s}$. Comparison of Figs. 7 and 8 shows that the second solution enhances active power sharing accuracy, while the second method enables sharing of reactive power according to the output rms current of the DERs. Specifically, when the DER1 power is increased from 200W to 1500W at *t=15s*, its reactive power generation is decreased below that of DERs 2-4 (see Figs. 8(a), (b)).

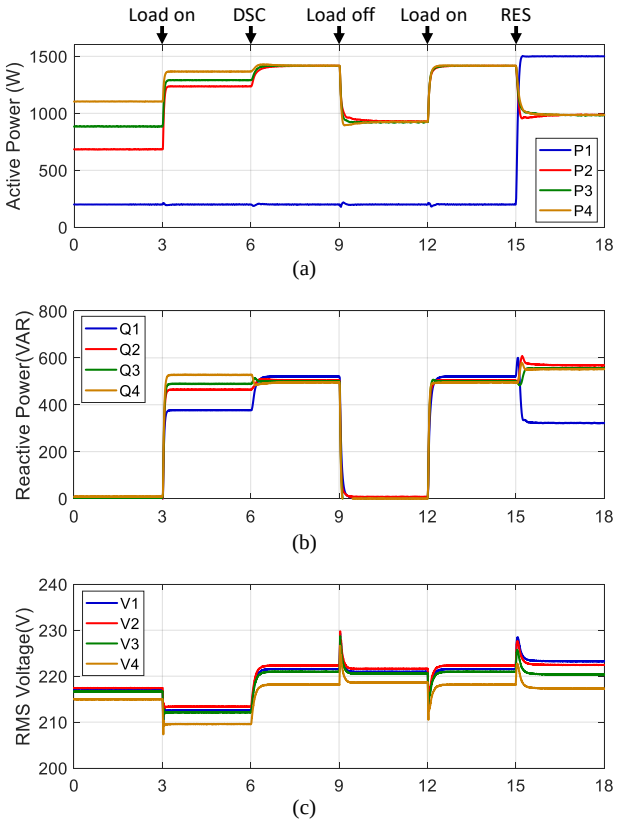

Fig. 8. Performance of control method B: a) active powers, b) reactive powers, c) rms voltages,

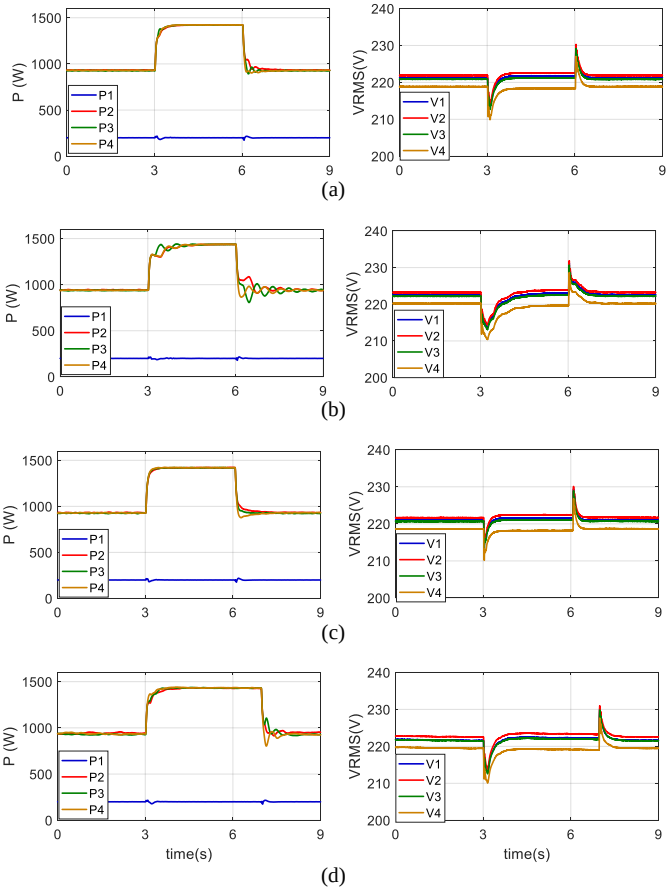

Fig. 9. Effect of communication constraints on the dynamic performance of the proposed method: a) time delay of 50ms, b) time delay of 200ms, c) packet loss of 50%, d) packet loss of 90%.

C. *Effect of Communication Constraints*

In this case study, the effect of communication constraints, including latency and packet loss, on the dynamic response of the proposed method is investigated with load 2 being turned off and on at $t = 3$s and $t = 6$ s, respectively. The DERs active power outputs and voltages subject to communication delays of 50ms and 200ms and packet losses of 50% and 90% are illustrated in Figs. 9(a)-(d), respectively. The results show that if the time delay and packet loss are less than 50ms and 50%, the effect of communication constrains on the proposed method is negligible. Although under severe conditions, the settling time and ringing are increased, the transient active powers and voltages remain within the safe operating region.

D. *Plug and Play Capability*

In the last case study, plug'n'play capability of the proposed control method is examined. To that end, the electrical connection of DER4 and accordingly all related communication links are disconnected at $t = 2s$. As illustrated in Fig. 10, the active and reactive power generations of DER1-3 are smoothly increased to compensate for the disconnection of DER4. Moreover, the voltages are maintained within an acceptable range of the rated value. Once the DER4 is reconnected at $t = 4s$, the powers and voltages are smoothly returned to their initial value. Although DER4 is disconnected from the MG, its reference frame remains synchronized with the grid thanks to the GPS synchronization technology. This facilitates the reconnection of unit 4 and ensures a smooth reconnection at $t = 6s$. This case study demonstrates the capability of the proposed method for smooth connection/disconnection of a DER to/from the MG. Opposed to the conventional distributed secondary control methods, no additional synchronization mechanisms e.g., PLL is required.

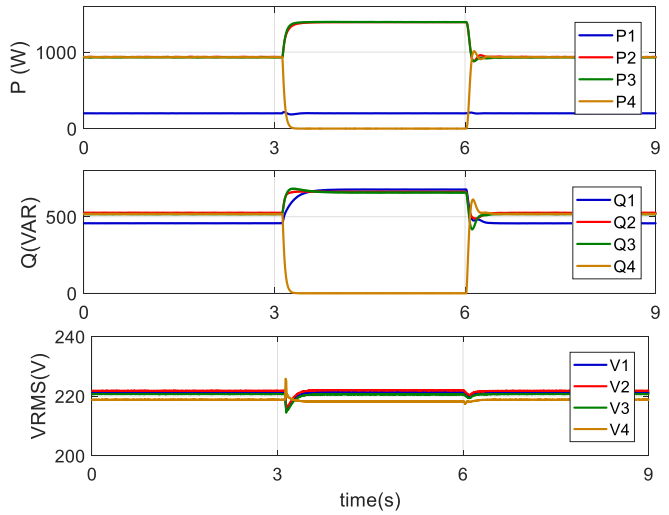

Fig. 10. Plug and play capability of the proposed method.

VII. Conclusions

In this paper, a new distributed control framework is proposed for low voltage resistive MGs. The proposed scheme is developed based on the physical characteristics of inverter-based MGs, including lack of inertia, low X/R of the network impedance, susceptibility of the DERs to overcurrent and distributed nature of the network. Specifically, by integrating GPS timing technology in the DER controllers, an inertia-free

voltage-current based droop control scheme is realized to achieve fast sharing of load current while maintaining the frequency at the rated value. The distributed secondary control method compensates the voltage deviations caused by the droop controller while facilitating accurate load sharing among the DERs. By adjusting the reactive power output of each unit according to its rms current output, the heavily loaded DERs are protected against overcurrent stresses. The proposed solution features plug-and-play functionality without any need for PLL synchronization mechanism. A mathematical model of the proposed method is formulated in state-space and eigenvalue analysis is carried out to demonstrate the small signal stability. Finally, experimental results are presented to demonstrate the efficacy of the proposed method in spite of communication constrains.

REFERENCES

[1] A. Purvins *et al.*, "A European supergrid for renewable energy: local impacts and far-reaching challenges," *Journal of Cleaner Production*, vol. 19, no. 17–18, pp. 1909-1916, 11 2011.

[2] M. S. Golsorkhi and D. D. C. Lu, "A Control Method for Inverter-Based Islanded Microgrids Based on V-I Droop Characteristics," *IEEE Trans. Power Del.*, vol. 30, no. 3, pp. 1196-1204, Jun. 2015.

[3] B. B. Johnson, S. V. Dhople, A. O. Hamadeh, and P. T. Krein, "Synchronization of Parallel Single-Phase Inverters With Virtual Oscillator Control," *IEEE Trans. Power Electron.*, vol. 29, no. 11, pp. 6124-6138, 2014.

[4] K. T. Tan, X. Y. Peng, P. L. So, Y. C. Chu, and M. Z. Q. Chen, "Centralized Control for Parallel Operation of Distributed Generation Inverters in Microgrids," *IEEE Trans. Smart Grid*, vol. 3, no. 4, pp. 1977-1987, Dec. 2012.

[5] Q. Shafiee, J. M. Guerrero, and J. C. Vasquez, "Distributed Secondary Control for Islanded Microgrids-A Novel Approach," *IEEE Trans. Power Electron.*, vol. 29, no. 2, pp. 1018-1031, Feb. 2014.

[6] A. Bidram and A. Davoudi, "Hierarchical Structure of Microgrids Control System," *IEEE Trans. Smart Grid*, vol. 3, no. 4, pp. 1963-1976, May 2012.

[7] A. G. Tsikalakis and N. D. Hatziargyriou, "Centralized Control for Optimizing Microgrids Operation," *IEEE Transactions on Energy Conversion*, vol. 23, no. 1, pp. 241-248, 2008.

[8] A. Bernstein, L. Reyes-Chamorro, J.-Y. Le Boudec, and M. Paolone, "A composable method for real-time control of active distribution networks with explicit power setpoints. Part I: Framework," Electric Power Systems Research, vol. 125, pp. 254-264, 2015.

[9] J. M. Guerrero, M. Chandorkar, T. Lee, and P. C. Loh, "Advanced Control Architectures for Intelligent Microgrids ; Part I: Decentralized and Hierarchical Control," *IEEE Trans. Ind. Electron.*, vol. 60, no. 4, pp. 1254-1262, April 2013.

[10] M. A. Mahmud, M. J. Hossain, H. R. Pota, and A. M. T. Oo, "Robust Nonlinear Distributed Controller Design for Active and Reactive Power Sharing in Islanded Microgrids," *IEEE Transactions on Energy Conversion*, vol. 29, no. 4, pp. 893-903, Dec. 2014.

[11] A. Bidram, A. Davoudi, F. L. Lewis, and S. S. Ge, "Distributed Adaptive Voltage Control of Inverter-Based Microgrids," *IEEE Transactions on Energy Conversion*, vol. 29, no. 4, pp. 862-872, Oct. 2014.

[12] V. Nasirian, S. Moayedi, A. Davoudi, and F. L. Lewis, "Distributed cooperative control of dc microgrids," *IEEE Trans. Power Electron.*, vol. 30, no. 4, pp. 2288-2303, 2015.

[13] C. W. F. Guo, J. Mao and Y.-D. Song, "Distributed Secondary Voltage and Frequency Restoration Control of Droop-Controlled Inverter-Based Microgrids," *IEEE Trans. Ind. Electron.*, vol. vol. 62, no. 7, pp. 4355–4364, July 2015.

[14] J. W. Simpson-Porco, Q. Shafiee, F. Dorfler, J. C. Vasquez, J. M. Guerrero, and F. Bullo, "Secondary Frequency and Voltage Control of Islanded Microgrids via Distributed Averaging," *IEEE Trans. Ind. Electron.*, vol. 62, no. 11, pp. 7025-7038, Nov. 2015.

[15] H. Cai and G. Hu, "Distributed Nonlinear Hierarchical Control of AC Microgrid via Unreliable Communication," *IEEE Trans. Smart Grid*, vol. 9, no. 4, pp. 2429-2441, July 2018.

[16] N. M. Dehkordi, N. Sadati, and M. Hamzeh, "Distributed Robust Finite-Time Secondary Voltage and Frequency Control of Islanded Microgrids," IEEE Transactions on Power Systems, vol. 32, no. 5, pp. 3648-3659, Sept. 2017.

[17] N. M. Dehkordi, N. Sadati, and M. Hamzeh, "Fully Distributed Cooperative Secondary Frequency and Voltage Control of Islanded Microgrids," *IEEE Transactions on Energy Conversion*, vol. 32, no. 2, pp. 675-685, June 2017.

[18] X. Wu and C. Shen, "Distributed Optimal Control for Stability Enhancement of Microgrids With Multiple Distributed Generators," IEEE Transactions on Power Systems, vol. 32, no. 5, pp. 4045-4059, Sept. 2017.

[19] E. Dall'Anese and A. Simonetto, "Optimal Power Flow Pursuit," *IEEE Trans. Smart Grid*, vol. 9, no. 2, pp. 942-952, March 2018.

[20] K. Baker, A. Bernstein, E. Dall'Anese, and C. Zhao, "Network-Cognizant Voltage Droop Control for Distribution Grids," *IEEE Transactions on Power Systems*, vol. 33, no. 2, pp. 2098-2108, March 2018.

[21] M. S. Sadabadi, Q. Shafiee, and A. Karimi, "Plug-and-Play Voltage Stabilization in Inverter-Interfaced Microgrids via a Robust Control Strategy," *IEEE Transactions on Control Systems Technology*, vol. 25, no. 3, pp. 781-791, May 2017.

[22] V. Nasirian, Q. Shafiee, J. M. Guerrero, F. L. Lewis, and A. Davoudi, "Droop-Free Distributed Control for AC Microgrids," *IEEE Trans. Power Electron.*, vol. 31, no. 2, pp. 1600-1617, March 2016.

[23] L. Lin-Yu and C. Chia-Chi, "Consensus-Based Droop Control Synthesis for Multiple DICs in Isolated Micro-Grids," *IEEE Trans. Power Syst.*, vol. 30, no. 5, pp. 2243-2256, 2015.

[24] M. S. Golsorkhi, D. D. C. Lu, Q. Shafiee, and J. M. Guerrero, "Distributed voltage control and load sharing for inverter-interfaced microdrid with resistive lines," in *2016 IEEE Energy Conversion Congress and Exposition (ECCE)*, 2016, pp. 1-7.

[25] M. S. Golsorkhi and D. D. C. Lu, "A Decentralized Control Method for Islanded Microgrids Under Unbalanced Conditions," *IEEE Trans. Power Del.*, vol. 31, no. 3, pp. 1112-1121, Jun. 2016.

[26] M. S. Golsorkhi and D. D. C. Lu, "A decentralized negative sequence compensation method for islanded mirogrids," in *Proc. International Symposium on Power Electronics for Distributed Generation Systems (PEDG)*, 2015, pp. 1-7.

[27] M. S. Golsorkhi, D. D. Lu, and J. M. Guerrero, "A GPS-Based Decentralized Control Method for Islanded Microgrids," *IEEE Trans. Power Electron.*, vol. 32, no. 2, pp. 1615-1625, Feb. 2017.

[28] M. S. Golsorkhi and D. D. C. Lu, "A decentralized power flow control method for islanded microgrids using V-I droop," in *Proc. Iranian Conference on Electrical Engineering (ICEE)*, 2014, pp. 604-609.

[29] A. Engler and N. Soultanis, "Droop control in LV-grids," in *Future Power Systems, 2005 International Conference on*, 2005, pp. 6 pp.-6.

[30] J. M. Guerrero, J. Matas, V. Luis Garcia de, M. Castilla, and J. Miret, "Decentralized Control for Parallel Operation of Distributed Generation Inverters Using Resistive Output Impedance," *IEEE Trans. Ind. Electron.*, vol. 54, no. 2, pp. 994-1004, Apr. 2007.

[31] M. Savaghebi, A. Jalilian, J. C. Vasquez, and J. M. Guerrero, "Secondary Control for Voltage Quality Enhancement in Microgrids," *IEEE Trans. Smart Grid*, vol. 3, no. 4, pp. 1893-1902, Jul. 2012.

[32] Y. A. R. I. Mohamed and E. F. El-Saadany, "Adaptive Decentralized Droop Controller to Preserve Power Sharing Stability of Paralleled Inverters in Distributed Generation Microgrids," *IEEE Trans. Power Electron.*, vol. 23, no. 6, pp. 2806-2816, Nov. 2008.

[33] M. S. Golsorkhi, M. Savaghebi, D. D.-C. Lu, J. M. Guerrero, and J. C. Vasquez, "A GPS-Based Control Framework for Accurate Current Sharing and Power Quality Improvement in Microgrids," IEEE Trans. Power Electron., vol. 32, no. 7, pp. 5675-5687, Jul. 2017.

[34] R. Olfati-Saber, J. A. Fax, and R. M. Murray, "Consensus and Cooperation in Networked Multi-Agent Systems," *Proceedings of the IEEE*, vol. 95, no. 1, pp. 215-233, Jan. 2007.

[35] J. Schiffer, T. Seel, J. Raisch, and T. Sezi, "Voltage Stability and Reactive Power Sharing in Inverter-Based Microgrids With Consensus-Based Distributed Voltage Control," *IEEE Trans. Control Syst. Technol.*, vol. 24, no. 1, pp. 96-109, Jan. 2016.

[36] A. Luo, Y. Chen, Z. Shuai, and C. Tu, "An Improved Reactive Current Detection and Power Control Method for Single-Phase Photovoltaic Grid-Connected DG System," *IEEE Transactions on Energy Conversion*, vol. 28, no. 4, pp. 823-831, 2013.

[37] M. S. Golsorkhi Esfahani, "Coordinated Control of Distributed Energy Resources in Islanded Microgrids," 2016.

[38] E. A. A. Coelho *et al.*, "Small-Signal Analysis of the Microgrid Secondary Control Considering a Communication Time Delay," *IEEE Trans. Ind. Electron.*, vol. 63, no. 10, pp. 6257-6269, 2016.

[39] E. Jarlebring, "The spectrum of delay-differential equations: numerical methods, stability and perturbation," Ph.D. dissertation, , Inst. Comp. Math, TU Braunschweig, Braunschweig, Germany, 2008.
[40] M. S. Golsorkhi, D. J. Hill, and H. R. Karshenas, "Distributed Voltage Control and Power Management of Networked Microgrids," *IEEE Journal of Emerging and Selected Topics in Power Electronics*, early access article, 2018.
[41] Microgrid Research programme", URL: www.microgrids.et.aau.dk.
[42] http://spectracom.com. *SecureSync Time & Frequency Reference System*. Available: http://spectracom.com/products-services/precision-timing/securesync-time-and-frequency-reference-system

Mohammad S. Golsorkhi (S13), (M' 16) received the B.Sc. (Hons.) degree from Isfahan University of Technology, Isfahan, Iran, in 2009, the M.Sc. (Hons.) degree from Tehran Poly technique, Tehran, Iran, in 2012, and the PhD degree from The University of Sydney, Sydney, Australia, in 2016, all in electrical engineering. During 2015, he was a visiting PhD student with the Department of Energy Technology, Aalborg University, Denmark. In 2016, he worked in The University of Hong Kong, Hong Kong as a postdoctoral fellow. Since 2017, he has been with the Department of Electrical and Computer Engineering, Isfahan University of Technology, Isfahan, Iran, where he is an Assistant Professor. His current research interests include control of micrograms, multi-microgird systems, integration of renewable energy resources into distribution networks, and power electronics.

Qobad Shafiee (S'13–M'15–SM'17) received PhD degree in electrical engineering from the Department of Energy Technology, Aalborg University, Aalborg, Denmark, in 2014. In 2014, he was a Visiting Scholar with the Electrical Engineering Department, the University of Texas at Arlington, Arlington, TX, USA. He was a Post-Doctoral Fellow with the Department of Energy Technology, Aalborg University, in 2015. He is currently an Assistant Professor, the Co-Leader of the Smart/Micro Grids Research Center at the University of Kurdistan, Sanandaj, Iran, where he was a lecturer from 2007 to 2011. His current research interests include modeling, energy management, control of power electronics-based systems and microgrids, and model predictive and optimal control of modern power systems

Dylan Dah-Chuan Lu (M'04–SM'09) received his B.E. and Ph.D. degrees, both in electronic and information engineering, from the Hong Kong Polytechnic University, Hong Kong, in 1999 and 2004 respectively. In 2003, he joined Power^{e}Lab Ltd. as a Senior Design Engineer where he was responsible for industrial switching power supply projects. He was a full-time faculty member with The University of Sydney from 2006 to 2016, where he now holds an Honorary position. Since July 2016, he has been an Associate Professor at the School of Electrical and Data Engineering, University of Technology Sydney, Australia. His current research interest includes efficient and reliable power conversion for renewable sources, energy storage systems, and microgrids. He is a Senior Member of IEEE and a Member of Engineers Australia. He was a recipient of the Best Paper Award in the category of Emerging Power Electronic Technique at the *IEEE PEDS* 2015. He is presently serving as an Associate Editor of the *IEEE Transactions on Circuits and Systems II: Express Briefs* and a Subject Editor of the *IET Renewable Power Generation*.

Josep M. Guerrero (S'01-M'04-SM'08-FM'15) received the B.S. degree in telecommunications engineering, the M.S. degree in electronics engineering, and the Ph.D. degree in power electronics from the Technical University of Catalonia, Barcelona, in 1997, 2000 and 2003, respectively. Since 2011, he has been a Full Professor with the Department of Energy Technology, Aalborg University, Denmark, where he is responsible for the Microgrid Research Program (www.microgrids.et.aau.dk). From 2014 he is chair Professor in Shandong University; from 2015 he is a distinguished guest Professor in Hunan University; and from 2016 he is a visiting professor fellow at Aston University, UK, and a guest Professor at the Nanjing University of Posts and Telecommunications.

His research interests is oriented to different microgrid aspects, including power electronics, distributed energy-storage systems, hierarchical and cooperative control, energy management systems, smart metering and the internet of things for AC/DC microgrid clusters and islanded minigrids; recently specially focused on maritime microgrids for electrical ships, vessels, ferries and seaports. Prof. Guerrero is an Associate Editor for a number of IEEE TRANSACTIONS. He has published more than 450 journal papers in the fields of microgrids and renewable energy systems, which are cited more than 30,000 times. He received the best paper award of the IEEE Transactions on Energy Conversion for the period 2014-2015, and the best paper prize of IEEE-PES in 2015. As well, he received the best paper award of the Journal of Power Electronics in 2016. During five consecutive years, from 2014 to 2018, he was awarded by Thomson Reuters as Highly Cited Researcher. In 2015 he was elevated as IEEE Fellow for his contributions on "distributed power systems and microgrids."